Carbohydrate Polymers 117 (2015) 201–210

Contents lists available at ScienceDirect

Carbohydrate Polymers

journal homepage: www.elsevier.com/locate/carbpol

Synthesis and characterization of amphiphilic photocleavable polymers based on dextran and substituted-ε-caprolactone

Ren-Shen Lee*, You-Chen Li, Shiu-Wei Wang

Division of Natural Science, Center of General Education, Chang Gung University, 259 Wen-Hwa 1st Road, Kwei-Shan, Tao-Yuan 333, Taiwan

ARTICLE INFO

Article history:
Received 20 August 2014
Received in revised form
17 September 2014
Accepted 24 September 2014
Available online 2 October 2014

Keywords:
Amphiphilic
Photocleavable
O-nitrobenzyl alcohol
Polysaccharide
Cellular uptake

ABSTRACT

In this study, we synthesized photocleavable amphiphilic block copolymers containing photodegradable linkers, 5-hydroxy-2-nitrobenzyl alcohol, as junction points between hydrophilic dextran (or maltodextrin) and hydrophobic poly(4-substituted-ε-caprolactone) chains, by using a combination of ring-opening polymerization and nucleophilic substitution reactions. When the polymer solutions were exposed to ultraviolet (UV) irradiation, major structural and morphological changes were observed in the particles. The copolymers were biodegradable and biocompatible, and they can self-assemble into spherical photoresponsive micelles. Fluorescence emission measurements indicated the release of Nile red, a hydrophobic dye, encapsulated by the Dex-ONB-PXCL micelles, in response to irradiation caused by the disruption of the micelles. Light-triggered bursts were observed for indomethacin (IMC)-loaded Dex-ONB-PXCL micelles during the first 5 h. The nanoparticles were associated with nonsignificant toxicity at concentrations of less than 100 μg mL^{-1}. The confocal microscopy and flow cytometry results showed that the uptake of DOX-loaded micelles by HeLa cells was slightly less than that of free DOX, and it was predominantly retained in the cytoplasm.

1. Introduction

During the past decade, the design of block copolymer (BCP) micelles, for which the assembly state in aqueous solution can be controlled or disrupted by applying light, has been researched extensively (Bertrand, Poggi, Gohy, & Fustin, 2014; Schumers, Fustin, & Gohy, 2010; Wang, Chen, Yang, Yang, & Liu, 2014). The growing interest in this research field is driven by the potential application of such BCP micelles as nanocarriers for the light-triggered release of guest molecules, which allows them to be remotely controlled, as well as their temporal and spatial selectivity. Various types of photo-responsive micelle can be designed depending on the type of the photo-responsive group and its location in the formed micelles. For example, photo-responsive molecules can be in principle either introduced in the micellar core, micellar corona, or at the core-corona interface, although they have been mainly incorporated into the micellar core. Photoresponsive molecules can respond in a reversible or irreversible manner when light is applied (Gohy & Zhao, 2013; Li, Zhang, Weng, Chen, & Liu, 2014). Recently, several research groups have demonstrated an irreversible response, involving the incorporation of the photocleavable units in the main-chain of one of the blocks, which induces the selective degradation of a specific micellar compartment. Among the many photolabile groups that have been studied, o-nitrobenzyl (ONB) alcohol derivatives have received considerable attention in the area of synthetic polymer and material science (Liu & Dong, 2012; Peng, Wang, Hua, & Lee, 2013; Schumers, Gohy, & Fustin, 2010; Zhao et al., 2013).

A drawback of polyethylene glycol (PEG)-based BCPs is the absence of reactive groups at their molecular chains, which limits further modification or ligand-coupling. By contrast, naturally occurring polysaccharides such as cellulose, dextran (Dex), and maltodextrin (MDex) exhibiting good hydrophilicity, biocompatibility, and biodegradability may be a suitable alternative to PEG hydrophilic segments for designing amphiphilic block copolymers (Bosker et al., 2003; Houga et al., 2009; Liu & Zhang, 2007; Otsuka et al., 2010). Dextrans consist of α (1→6) linked glucosyl units and maltodextrins of α (1→4) linked glucosyl units. However, few studies have examined polysaccharide-based block copolymers (Hernandez, Soliman, & Winnik, 2007; Peng et al., 2011; Xu, Lu, Du, & Li, 2007).

In this report, we describe the synthesis of an easily cleavable Dex-ONB-PXCL with ultraviolet (UV) irradiation, in which a photochemically sensitive ONB group is installed as a linker. The desired amphiphilic ONB-linked Dex-b-PXCL copolymers (Dex-ONB-PXCL) were synthesized on Dex or MDex as a hydrophilic block

* Corresponding author. Tel.: +886 3 2118800x5054; fax: +886 3 2118700.
E-mail address: shen21@mail.cgu.edu.tw (R.-S. Lee).

http://dx.doi.org/10.1016/j.carbpol.2014.09.062
0144-8617/

and poly(4-methyl-ε-caprolactone) (PMCL) or poly(4-phenyl-ε-caprolactone) (PBCL) as a hydrophobic block by ring-opening polymerization (ROP) and nucleophilic substitution reaction. To our knowledge, no information is available on amphiphilic photocleavable block copolymers comprising polysaccharide and biodegradable polyester segments. The physicochemical and photodegradable properties of these micelles in the aqueous phase were examined by fluorescence spectroscopy, dynamic light scattering (DLS), and transmission electron microscopy (TEM). The fluorescent imaging and cytotoxicity study of these DOX-encapsulated polymeric micelles were internalized into human cervical cancer HeLa cells to demonstrate their potential as fluorescent probes in optical bio-imaging.

2. Experimental

2.1. Materials

4-Methylcyclohexanone, 4-phenylcyclohexanone, dextran (M_n 1500 Da), maltodextrin (M_n approximately 2700 Da), 5-hydroxy-2-nitrobenzyl alcohol, 3-bromo-propanol, pyrene, indomethacin (IMC), and Nile red (NR) were purchased from Aldrich Chemical Co. (Milwaukee, WI). *m*-Chloroperoxybenzoic acid was purchased from Fluka Chemical Co. (Buchs SG1, Switzerland). Stannous octoate ($SnOct_2$) was purchased from Strem Chemical Inc. (Newburyport, MA). 3-Bromo-propyl-dextran, 3-bromo-propyl-maltodextrin, 4-methyl-ε-caprolactone (MCL) and 4-phenyl-ε-caprolactone (BCL) were prepared according to methods described previously with modifications (Cai, Jiang, Shen, & Fan, 2012; Kang & Moon, 2009; Peng, Wang, & Lee, 2013). Doxorubicin hydrochloride (99%) (Aldrich, Saint Louis, MO) was deprotonated to obtain hydrophobic DOX as described previously (Kuang et al., 2012). N,N-dimethyl formamide (DMF), and toluene were distilled under calcium hydride. Other high-pressure liquid chromatography (HPLC) grade solvents, such as tetrahydrofuran (THF), dimethylsulfoxide (DMSO), methanol, chloroform ($CHCl_3$), and *n*-hexane, were purchased from Merck (Darmstade, Germany). A Milli-Q Plus system (Waters, Milford, MA) was used to obtain ultrapure water. Dulbecco's modified Eagle's medium (DMEM), trypsin/EDTA, 100× antibiotic-antimycotic, and Hoechst 33342 nuclei dye were purchased from Gibco, Invitrogen Corp. (Carlsbad, CA). Fetal bovine serum (FBS) was obtained from Biological Industry (Kibbutz Beit Haemek, Israel). A CellTiter 96® AQueuous One Solution kit was obtained from Promega (Fitchburg, Wisconsin) Amiloride, chlorpromazine, methyl-β-cyclodextrin, and nystatin were purchased from Sigma–Aldrich (St. Louis, MO).

2.2. Synthesis of Dex-ONB-PXCL diblock copolymers

All glassware was dried in an oven and handled under a dry nitrogen stream. The polymerization reaction to create Dex_{10}-ONB-$PMCL_{34}$ proceeded as follows: 5-hydroxy-2-nitrobenzyl alcohol (62.6 mg, 0.37 mmol), as an initiator, and MCL (1.39 g, 14.8 mmol) were introduced into a flask, heated under a dry nitrogen stream, and dissolved in 50 mL of toluene. Subsequently, 22 mg of $SnOct_2$ (1.5 wt% based on the weight of ONB and MCL) was added to the flask. The flask was purged with nitrogen and refluxed for 24 h, and the solution was vacuum-concentrated under reduced pressure. The resulting product (HONB-$PMCL_{34}$) was dissolved in $CHCl_3$, and precipitated into excess *n*-hexane/diethyl ether (v/v, 5:1) while stirring. The purified polymer was dried in vacuo at 50 °C for 24 h and then analyzed. Fig. 1A shows a representative ^{1}H nuclear magnetic resonance (^{1}H NMR) spectrum of HONB-$PMCL_{34}$, and Fig. S1A (in supporting information) shows a representative Fourier transform infrared (FT-IR) spectrum of HONB-$PMCL_{34}$. The resonance peaks were assigned to the corresponding hydrogen atoms of HONB-$PMCL_{34}$. Subsequently, a mixture of HONB-$PMCL_{34}$ (0.95 g, 0.22 mmol, 1 equiv., M_n = 4250 g mol^{-1}) and potassium carbonate (92.4 mg, 0.66 mmol, 3 equiv.) was stirred in dimetylformamide (DMF) (10 mL) for 60 min at 60 °C. 3-Bromo-propyl-dextran (Dex-$CH_2CH_2CH_2Br$, 0.67 g, 0.26 mmol, 1.2 equiv., M_n = 2490 g mol^{-1}) in DMF (5 mL) was added, and the mixture was stirred for 24 h at 60 °C. After filtration, the filtrate was put into a dialysis tube with molecular weight cut-off (MWCO) of 1000 Da (Cellu·Sep H1, Membrane Filtration Products, Inc., Seguin, TX) and dialyzed against DMF for 24 h, followed by precipitation into excess diethyl ether while stirring. The purified polymer (Dex_{10}-ONB-$PMCL_{34}$) was dried in vacuo at 50 °C for 24 h and then analyzed. Fig. 1B shows a representative ^{1}H NMR spectrum of Dex_{10}-ONB-$PMCL_{34}$, and Fig. S1C (in supporting information) shows a representative FT-IR spectrum of Dex_{10}-ONB-$PMCL_{34}$.

2.3. Ultraviolet irradiation

Dex_{10}-ONB-$PMCL_{34}$ polymer (1.5 mg) in inhibitor-free tetrahydrofuran (THF) (1 mL) or polymer micelles in phosphate buffer solution (PBS) (0.1 M, pH 7.4) were exposed to UV light from a UV light system (model PR-2000, Phnchum Co., Taiwan) equipped with a Hitachi FL8BL-B lamp (352 nm, 8 W × 8 W). To prevent UV absorption, the samples were placed in quartz cuvettes with a spot size of approximately 1 cm^2 and irradiated at room temperature for an assigned duration. Radiation was applied vertically from the top of the cuvette.

2.4. Preparation of polymeric micelles

Polymeric micelles of Dex-ONB-PXCL polymers were prepared using a dialysis. Briefly, a solution of Dex-ONB-PXCL polymer (30 mg) in DMF (5 mL) was placed in a dialysis bag with a molecular weight cutoff (MWCO) of 3500 Da and dialyzed against deionized water at an ambient temperature for 24 h. The water was replaced at 2 h intervals.

2.5. Determination of drug-loading content and drug entrapment efficiency

Dex_{10}-ONB-$PMCL_{34}$ (50-fold CMC value) was dissolved in 6 mL of methylene chloride by using oil-in-water evaporation. The anti-inflammatory drug indomethacin (IMC) was added to the polymer in a 1:1 weight ratio to serve as a model drug. The solution was added dropwise to 150 mL of distilled water containing 1 wt% poly(vinyl alcohol) and stirred vigorously. Poly(vinyl alcohol) was used as a surfactant to reduce micelle aggregation. Sonication was applied for 1 h at an ambient temperature to reduce the droplet size. The emulsion was stirred at an ambient temperature overnight to evaporate the methylene chloride. The unloaded IMC residue was removed by filtering through a Teflon filter (Whatman) with an average pore size of 0.45 μm, and the micelles were obtained by vacuum drying. A weighed amount of micelles was then disrupted by adding a 10-fold excess volume of DMF. Drug content was assayed spectrophotometrically at 320 nm using a diode array UV–vis spectrophotometer. The following equations were used to calculate the drug-loading content and drug entrapment efficiency:

$$\text{Drug-loading content}\,(\%) = \frac{\text{Weight of drug in the micelles}}{\text{Weight of micelles}} \times 100 \quad (1)$$

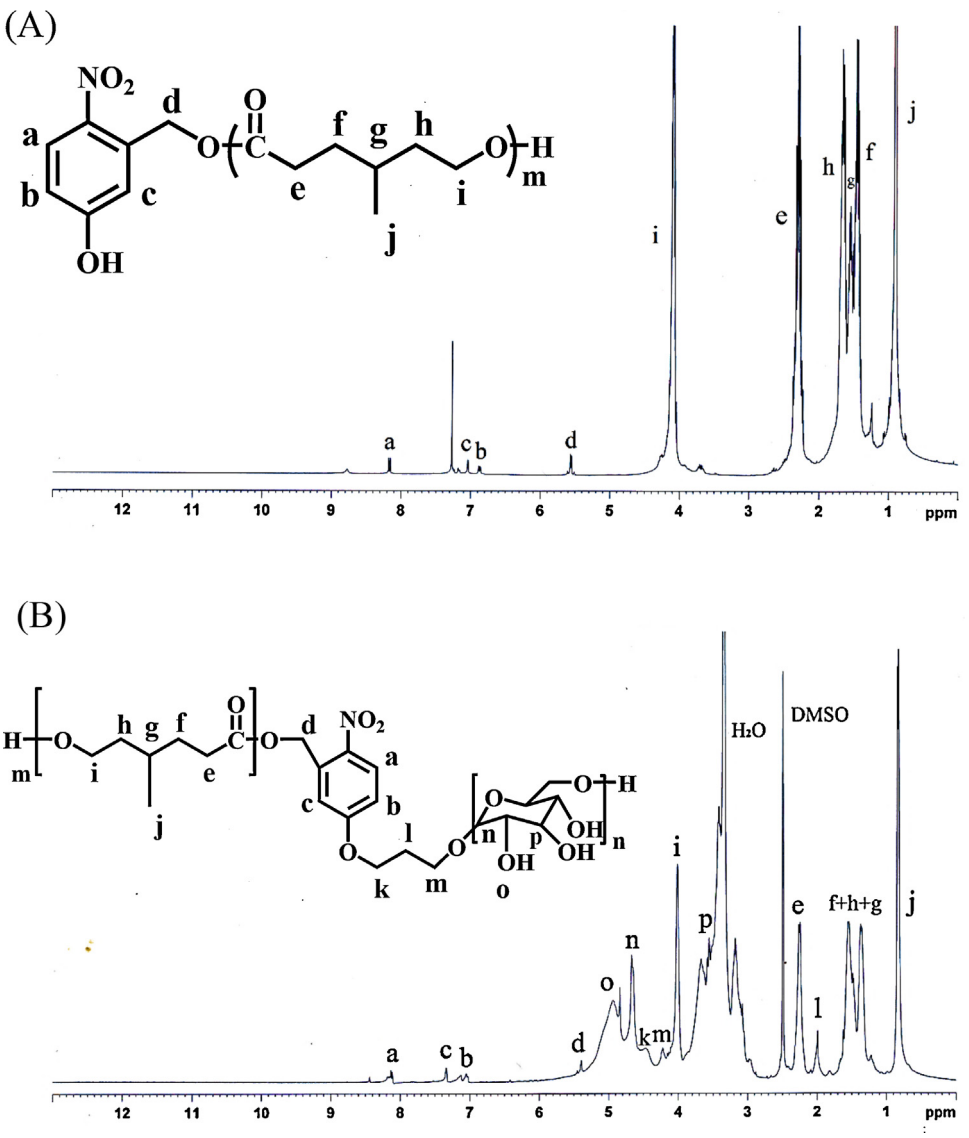

Fig. 1. Representative ^{1}H NMR spectroscopy (A) HONB-PMCL$_{34}$, (B) Dex$_{10}$-ONB-PMCL$_{34}$ in $CDCl_3$.

$$\text{Drug entrapment efficiency (\%)} = \frac{\text{Weight of drug in the micelles}}{\text{Weight of drug provided initially}} \times 100 \quad (2)$$

2.6. Analysis of in vitro drug release

Appropriate amounts of IMC-loaded micelles (110.2 mg) were weighed and suspended in 10 mL of PBS (0.1 M, pH 7.4). The micellar solution was introduced to a dialysis membrane bag (MWCO = 3500 Da), and the bag was placed in 50 mL of a PBS release medium. The medium was shaken (30 revolutions/min) or exposed to UV light at 37 °C. At predetermined intervals, 3 mL aliquots of the aqueous solution were withdrawn from the release medium, and an identical volume of fresh buffer solution was added. The concentration of released IMC was determined using a UV–vis spectrophotometer at a wavelength of 320 nm. The rate of controlled drug-release was measured according to the cumulatively released weight of IMC by using the calibration curve for IMC.

2.7. Determination in vitro cellular viability

The Promega CellTiter 96® AQueuous One Solution kit was used to determine cellular viability. The assay was performed according to the manufacturer's instructions with minor modifications. Briefly, HeLa cells were seeded in a 24-well plate (3×10^4 cells/well) overnight, and subsequently treated with various concentrations of polymers (or DMSO vehicles) added to DMEM/F12 1:1 medium with 1% FBS in a humidified 37 °C incubator supplied with 5% CO_2. After 48 h, the medium in each well was removed and replaced with 350 μL of warm PBS and 35 μL of CellTiter 96® AQueuous One Solution. Subsequently, the mixture was incubated at 37 °C for 4 h. After incubation, 110 μL of supernatant from each well was moved to a 96-well plate and absorbance was measured at 485 nm by using an ELISA reader (Hidex, Finland).

2.8. Flow cytometric analysis of the uptake of doxorubicin-loaded micelles

HeLa cells were seeded in 35-mm dishes (1.5×10^5 cells/dish) and cultured overnight. Subsequently, DOX-loaded Dex$_{10}$-ONB-PMCL$_{34}$ micelles and free DOX (447 ng mL^{-1}) dissolved in DMEM/F12 1:1 medium with 1% FBS, were added and incubated for 5 and 30 min. Cells were trypsinized and fixed with 4% paraformaldehyde for 15 min prior to analysis. A BD FACSCalibur flow cytometer (equipped with a 488-nm argon laser) and CellQuest software were used for the analysis. An FL2 channel

captured the fluorescence of the DOX. Each experiment was conducted in triplicate.

3. Results and discussion

3.1. Synthesis and characterization of Dex-ONB-PXCL block copolymer

Scheme 1 depicts the strategy for synthesizing the photocleavable Dex-ONB-PXCL copolymer. A difunctional initiator 5-hydroxy-2-nitrobenzyl alcohol, which contains two hydroxyl groups of benzyl and phenol, was chosen as the photo-responsive molecule because of its chemical stability and rapid cleavage in response to near-UV irradiation (wavelength >320 nm) (Griffin et al., 2013; Hu, Tian, Liu, Zhang, & Liu, 2013). First, the benzyl hydroxyl group initiated the ROP of ε-CL or 4-substituted-ε-caprolactone (MCL and BCL) catalyzed by $SnOct_2$. Nucleophilic substitution etherified the phenolic hydroxyl group of the resulting HONB-PXCL with Dex-$(CH_2)_3$Br or MDex-$(CH_2)_3$Br in DMF at 60 °C to provide the Dex-ONB-PXCL or MDex-ONB-PXCL polymer. Table 1 lists the coupling results. The $M_{n,GPC}$ was in agreement with $M_{n,NMR}$ and $M_{n,th}$. FT-IR and ^{1}H NMR results confirmed the effective coupling of Dex-$(CH_2)_3$Br or MDex-$(CH_2)_3$Br to provide the Dex-ONB-PXCL and MDex-ONB-PXCL. The representative ^{1}H NMR spectrum (Fig. 1B) indicated novel signals from Dex. The resonance peaks could be assigned to the corresponding hydrogen atoms of the Dex blocks at $\delta = 4.61$ (H_n, anomeric —C*H*—), 3.78–3.03 (H_p, —C*H*—). The resonance peaks of the PMCL blocks were observed at $\delta = 4.10$ (H_i, —CH_2O—), 2.30 (H_e, —CH_2—), 1.40–1.80 (H_{f+g+h}, —C*H*—, and —CH_2—), and 0.95 (H_j, —CH_3). The IR spectrum of the Dex-ONB-PXCL (Fig. S1C in supporting information) indicated typical carbonyl absorption of an ester of ONB-PXCl at 1720 cm^{-1}, and the broad peak H—O between 3600 and 3100 cm^{-1} as well as the C—O absorption at 1050 cm^{-1} for Dextran, respectively. Fig. S2 (in supporting information) shows the representative GPC curves of Dex_{10}-ONB-$PMCL_{34}$ compared with those of the original HONB-$PMCL_{34}$. The GPC traces indicate the unimodal distribution of Dex_{10}-ONB-$PMCL_{34}$ with a shift in the peak towards the higher molecular weight region, compared with that of the original HONB-$PMCL_{34}$. Attempt to couple longer dextran (M_n 6000 Da) with the same HONB-PXCL and using the same method were unsuccessful (data not shown).

Table 1 and Fig. S3 (in supporting information) show the thermal behaviors of the block copolymers and DSC curves of the Dex-ONB-PXCL, respectively. The Dex-ONB-PXCL copolymers exhibited amorphous T_g (except for the Dex-ONB-PCL series polymers). The DSC curves indicated that, fixing the length of the Dex block and increasing the length of the PXCL block caused a slightly decreased T_gs. When the M_n of the Dex was fixed at 1500 g mol^{-1} (Dex_{10}), the T_g decreased from −53.9 °C to −55.9 °C when the length of the PMCL block was increased from $PMCL_{26}$ to $PMCL_{55}$ because the flexibility of the PMCL block increased when larger amounts of MCL were incorporated into the macromolecular backbone.

3.2. Degradation of photolabile Dex-ONB-PXCL polymers

The photolytic degradation of the polymer was investigated by UV–vis spectroscopy, observing the spectral changes of a polymer solution over irradiation time. Accordingly, we dissolved 1.5 mg Dex_{10}-ONB-$PMCL_{34}$ in 1 mL inhibitor-free THF and then irradiated the solution using a UV lamp (352 nm, 8 W × 8 W) for a given duration. The experiment was conducted at an ambient temperature. The absorbance of the solution was recorded at various time points. In the UV–vis spectra (Fig. 2A), the typical behavior of ONB esters under irradiation was observed: the decrease of the band at 306 nm

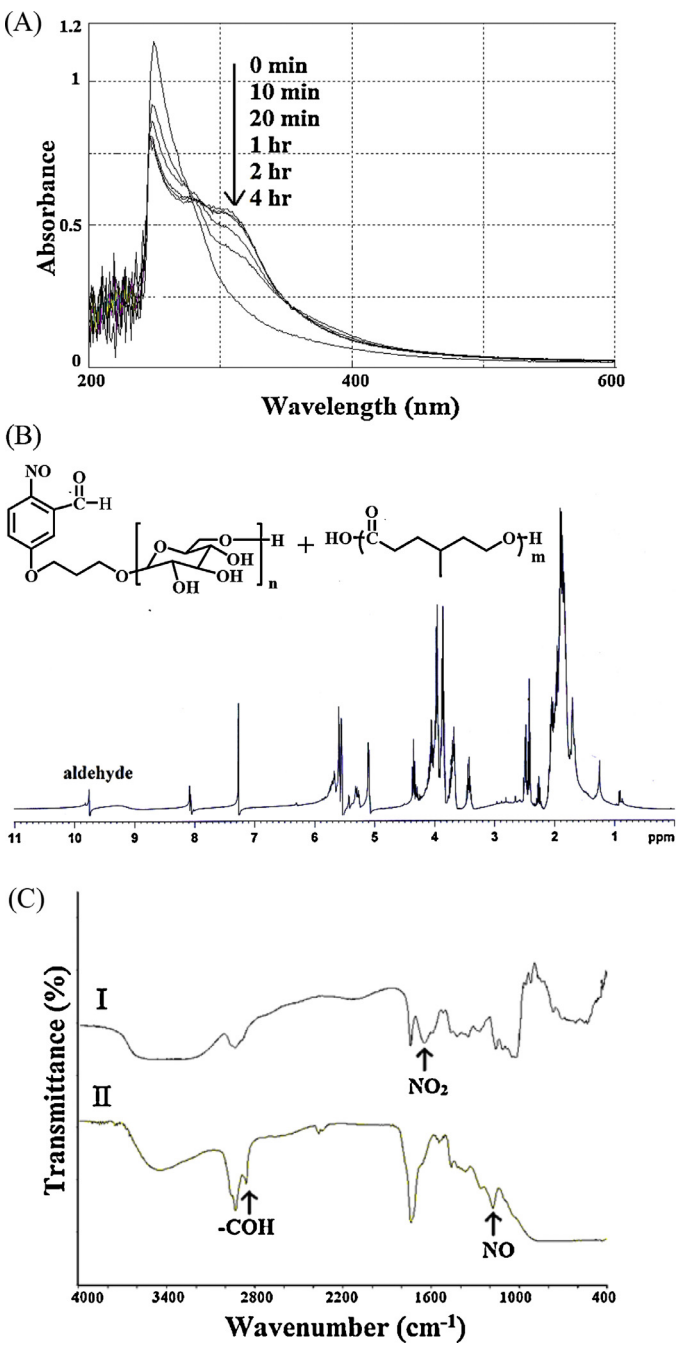

Fig. 2. (A) Time-dependent UV–vis spectral changes of Dex_{10}-ONB-$PMCL_{34}$ in THF (1.5 mg mL^{-1}), (B) ^{1}H NMR of Dex_{10}-ONB-$PMCL_{34}$ after UV irradiation in $CDCl_3$, (C) FT-IR of Dex_{10}-ONB-$PMCL_{34}$ before (I) and after (II) UV irradiation.

corresponded to the cleavage of the ONB ester functions with irradiation time and with the isosbestic points at 282 nm. In addition, the polymer solution changed from colorless to slightly yellow, which is typical of nitrosobenzaldehyde produced by photocleavage.

Additionally, photodegradation was followed by ^{1}H NMR and FT-IR. Marked changes in chemical shifts were observed (Fig. 2B). Upon degradation, the ester linkage between the ONB and PXCL was converted to aldehyde functionality (at approximately 9.78 ppm). The aromatic signals were also affected, because of the transition from a nitrobenzene to a nitrosobenzene structure, thus confirming the cleavage. The FT-IR (Fig. 2C) further confirmed the photodegradation; the absorption of NO_2 (ν1602 cm^{-1}) disappeared in favor of a new absorption at 1190 cm^{-1}, which is characteristic of

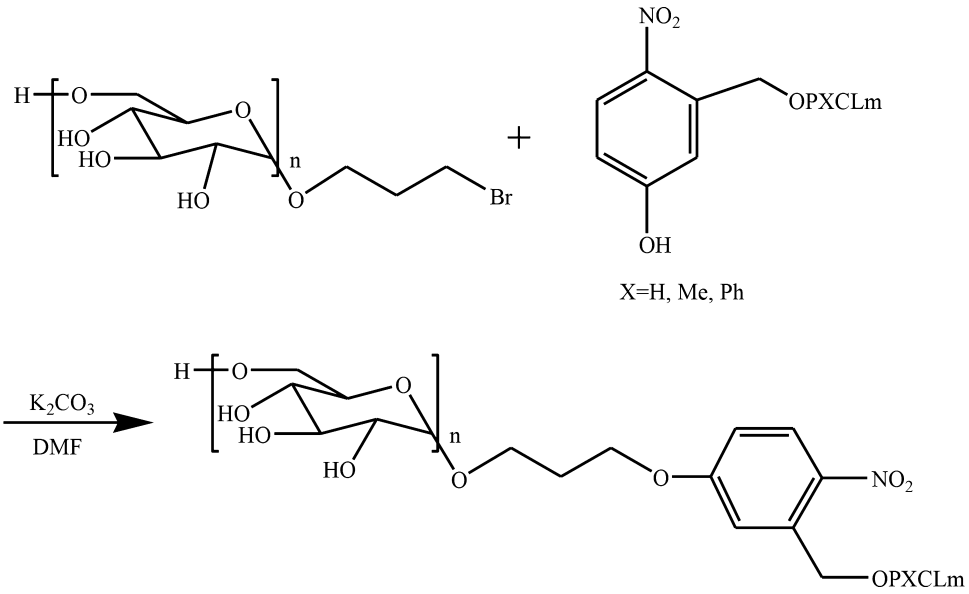

Scheme 1. Strategy for the synthesis of photocleavable Dex-ONB-PXCL copolymer.

the nitroso, and a new absorption of aldehyde functionality was observed at 2850 cm^{-1}.

3.3. Micelles of Dex-ONB-PXCL

The amphiphilic nature of Dex-ONB-PXCL polymers, which consist of hydrophilic Dex and hydrophobic ONB-PXCL segments, enables micelles to form in water. In this study, the characteristics of the Dex-ONB-PXCL micelles in the aqueous phase were investigated by using fluorescence techniques. The critical micelle concentrations (CMCs) of the Dex-ONB-PXCL in the aqueous phase were determined by using pyrene as a probe molecule. The fluorescence intensity of the excitation spectrum of pyrene (data not shown) increased in conjunction with the concentration of the Dex-ONB-PXCL polymer. The characteristic feature of the pyrene excitation spectrum, a red-shift of the (0,0) band from 331 to 335 nm during partitioning into a micellar hydrophobic core, to determine the CMC values of the Dex-ONB-PXCL polymers. Fig. S4 (supporting information) shows the intensity ratios I_{335}/I_{331} of pyrene excitation spectra vs. the logarithm of the Dex-ONB-PXCL polymers concentrations. The CMC was determined from the interaction of straight line segments drawn through the points of the lowest polymer concentrations, which lie on a nearly horizontal line, and the points of the rapidly rising region of the plot. Table 2 lists the CMC values of the various Dex-ONB-PXCL polymers. The Dex-ONB-PXCL polymers formed micelles in the aqueous phase, and the CMCs ranged from 2.2 to 50.4 mg L^{-1}. The Dex-ONB-PXCL polymers exhibited lower CMC values than those of the surfactant (e.g. 2.3 g L^{-1} for sodium dodecyl sulfate in water), indicating thermodynamically favorable self-association in the Dex-ONB-PXCL. Decreasing CMC values with increasing hydrphobicity of the hydrophobic segment or hydrophilicity of the hydrophilic segment were observed.

The mean hydrodynamic diameters of micelles incorporating IMC and blank micelles, ranged from 147.5 to 278.8 nm and from 87.3 to 189.7 nm, respectively. The micelles incorporating IMC were larger than the blank micelles because of the incorporation of the hydrophobic drug. The Dex-ONB-PXCL micelles were associated with a narrow distribution, with a polydispersity index (PDI) of less than 0.34. Fig. S5 (in supporting information) shows the spherical morphology of $MDex_7$-ONB-$PMCL_{26}$ micelles.

Table 1
Characteristics of the Dex-ONB-PXCL used in this study.

Polymer[a]	$M_{n,th}$[b]	$M_{n,NMR}$[c]	$M_{n,GPC}$[d]	M_w/M_n[d]	T_g (°C)[e]	T_m (°C)[e]
Dex_{10}-ONB-PCL_{11}	2923	1954	2030	1.24		51.7/54.9
Dex_{10}-ONB-PCL_{29}	4975	3305	3490	1.38		46.3/49.6
Dex_{10}-ONB-$PMCL_{26}$	4997	3223	2880	1.41	−53.9	
Dex_{10}-ONB-$PMCL_{34}$	6021	4939	5590	1.47	−55.9	
Dex_{10}-ONB-$PMCL_{55}$	8709	7830	6600	1.64	−55.5	
Dex_{10}-ONB-$PBCL_{27}$	6799	6445	3740	1.43	12.7	
Dex_{10}-ONB-$PBCL_{43}$	9839	7109	4700	1.71	12.9	
$MDex_7$-ONB-$PMCL_{26}$	4487	5118	3780	1.54	−53.8	
$MDex_7$-ONB-$PMCL_{55}$	8199	6127	5000	1.55	−55.9	
$MDex_{17}$-ONB-$PMCL_{55}$	9909	7959	6270	1.86		

[a] *Abbreviations*: Dex = Dextran (M_n = 1500 Da); ONB = 4-hydroxy-2-nitrobenzyl alcohol; $MDex_7$ = Maltodextrine$_7$ (dextrose equivalent 4.0–7.0; M_n = 990 Da); $MDex_{17}$ = Maltodextrine$_{17}$ (dextrose equivalent 13.0–17.0; M_n = 2700 Da); PCL = poly(ε-caprolactone); PMCL = poly(4-methyl-ε-caprolactone); PBCL = poly(4-phenyl-ε-caprolactone).

[b] $M_{n,th} = M_{n,HONB\text{-}PXCL} + M_{n,Dex}$ (where $M_{n,HONB\text{-}PXCL}$ is the number-average molecular weight of HONB-PXCL, $M_{n,Dex}$ is the number-average molecular weight of dextran).

[c] Determine by ^{1}H NMR spectroscopy of polymer.

[d] Determine by GPC.

[e] Determine from DSC thermograms for second run.

Table 2
Properties of IMC-loaded Dex-ONB-PXCL polymer micelles.

Polymer	CMC (mg L^{-1})	Drug loading content[a] (%)	Drug entrapment efficiency[a] (%)	Micelles size (nm)					
				Blank	PDI	Zeta potential (mV)	With IMC	PDI	Zeta potential (mV)
Dex_{10}-ONB-PCL_{11}	50.4	9.8	19.6	157.2 ± 60.1	0.15	−23.2			
Dex_{10}-ONB-PCL_{29}	39.1	10.3	20.6	189.7 ± 78.4	0.25	−27.3	191.3 ± 20.6	0.27	−0.5
Dex_{10}-ONB-$PMCL_{26}$	26.0	6.9	13.9	114.6 ± 73.7	0.21	−26.5	172.4 ± 94.9	0.27	−18.1
Dex_{10}-ONB-$PMCL_{34}$	6.9	8.7	17.4	87.3 ± 35.2	0.13	−35.9	147.5 ± 67.9	0.17	−17.9
Dex_{10}-ONB-$PMCL_{55}$	2.2	12.1	24.2	109.8 ± 9.0	0.23	−7.2	241.7 ± 36.7	0.31	−0.7
Dex_{10}-ONB-$PBCL_{27}$	9.4	9.4	18.7	112.0 ± 20.3	0.26	−7.0	169.5 ± 25.8	0.11	−23.1
Dex_{10}-ONB-$PBCL_{43}$	9.1	11.4	22.9	148.5 ± 42.0	0.26	−9.4	240.5 ± 92.9	0.24	−11.1
$MDex_7$-ONB-$PMCL_{26}$	27.8	22.0	44.0	156.7 ± 72.7	0.34	−30.6	269.3 ± 131.2	0.23	−7.4
$MDex_7$-ONB-$PMCL_{55}$	6.8	28.2	56.3	182.2 ± 20.7	0.27	−10.2	278.8 ± 91.1	0.31	−1.9
$MDex_{17}$-ONB-$PMCL_{55}$	14.3	5.9	11.9	61.2 ± 23.4	0.14	−2.9			

[a] Feed weight ratio IMC/polymer = 1/1.

When the drug was incorporated, the micelle size increased marginally (Fig. S5B, in supporting information). The diameters measured using DLS were similar to those estimated using the TEM images.

The micelle surfaces were negatively charged with comparable zeta potentials in the range of −2.9 to −35.9 mV (Table 2). IMC loading caused a lower degree of negative charges on the micellar surface because the hydroxyl groups of dextran were protoned by the carboxylic acid group in IMC. Less negative charged surface is favorable to prevent uptake by the phagocytic cells, which results in faster clearance from the blood (Yang et al., 2012).

3.4. Photocleavable behaviors of micelles

The photodegradation of the micelles was studied at various irradiation times by monitoring changes in NR fluorescence (Lv, Wang, Wang, & Tang, 2012). The reduction in NR fluorescence intensity at 556 nm was recorded. After dissolving the NR and Dex_{10}-ONB-$PMCL_{34}$ in THF (0.5 mg mL^{-1}, NR to polymer ratio ÷ 1:3), water was added to induce micelle formation and concomitant NR encapsulation by the micelle core. Subsequently, we removed the THF by evaporation and filtered the nonsolubilized NR by using microfiltration (0.2 μm pore filter). The final micelle concentration was adjusted to 0.2 mg mL^{-1}. Fig. 3A shows the fluorescence emission spectra of NR loaded in the Dex_{10}-ONB-$PMCL_{34}$ micelle before and after UV irradiation at various time intervals. Fig. 3B shows normalized fluorescence plotted against time; with UV irradiation of the solution, the emission intensity was reduced by less than 65% after 6 h of irradiation. The micelles exhibited photolabile properties in response to light activation. We used TEM to observe the morphologically changes after UV irradiation. Fig. 3C and D shows the images collected before and after UV irradiation (6 h). The TEM micrographs indicated distinct morphologies, confirming the rapid disintegration of the NR-loaded micelles in the aqueous solution. Prior to irradiation, the micelles were uniform in size. However, after exposure to UV light, broken micelles were observed, indicating that brief irradiation induced a changed assembly state. The observed rate of fluorescence quenching was rapid, indicating a burst release of loaded NR into the aqueous medium.

3.5. Evaluation of drug-loading content, entrapment efficiency and in vitro release of IMC

The drug loading content and drug entrapment efficiency of the polymeric micelles were determined by using UV–vis absorption spectroscopy. IMC, a widely used hydrophobic, non-steroidal, anti-inflammatory drug, was chosen as a model drug to investigate drug loading in the hydrophobic core. The maximal absorption peak of the IMC was proportional to its concentration at 320 nm. After releasing the IMC and removing the polymer precipitate, the amount of loaded IMC was determined by the absorbance at 320 nm. Table 2 lists the calculated drug-loading content and entrapment efficiency values. At a constant feed weight ratio (1:1), the maximal drug-loading content and entrapment efficiency was 12.1% and 24.2% for the Dex_{10}-ONB-PXCL series of polymers, and 28.2% and 56.3% for the MDex-ONB-PXCL series of polymers, respectively. Drug loading content and entrapment efficiency increased in conjunction with the hydrophilicity of the hydrophilic segment, or increasing hydrophobicity of the hydrophobic segment (Li, Wang, Wang, Wang, & Jiang, 2013).

The release rate was monitored by determining the concentration of the total amount of released drug. Fig. 4 shows the release profiles of the IMC from the IMC micelles of the Dex_{10}-ONB-$PMCL_{34}$ and $MDex_7$-ONB-$PMCL_{26}$. The IMC-loaded micelles of the Dex_{10}-ONB-$PMCL_{34}$ and $MDex_7$-ONB-$PMCL_{26}$ exhibited well-developed, sustained drug-released patterns. Compared with the released rated in the absence of UV irradiation, the release rate of the IMC was considerably more rapid under UV irradiation at 37 °C, with approximately 60% of the encapsulated IMC released in a sustained manner during the first 5 h. These results confirmed our hypothesis that burst release is achieved by the rapid disintegration of the Dex-ONB-PMCL micelle, in which core–shell degradation can be activated by removing a small number of light-trigger units (Han, Tong, & Zhao, 2011; Griffin et al., 2013; Zhao, Sterner, Coughlin, & Theato, 2012).

3.6. In vitro cytotoxicities of the polymer

The in vitro cytotoxicities of the Dex_{10}-ONB-$PMCL_{34}$ and $MDex_7$-ONB-$PMCL_{26}$ polymers were evaluated by using the 3-(4,5-dimethylthiazol-2-yl)-5-(3-carboxymethoxyphenyl)-2-(4-sulfophenyl)-2H-tetrazolium (MTS) assay in HeLa cells with various polymer concentrations. To eliminate any unwanted cytotoxic effects of the polymer, we assessed the viability of cells loaded with increasing amounts of Dex_{10}-ONB-$PMCL_{34}$ or $MDex_7$-ONB-$PMCL_{26}$ by using a Promega CellTiter 96® AQueuous One Solution kit. HeLa cells were incubated with various concentrations of Dex_{10}-ONB-$PMCL_{34}$ or $MDex_7$-ONB-$PMCL_{26}$ for 48 h before reaction with the MTS reagent, which is bioreduced by esterase in living cells to formazan, enabling spectrophotometric analysis absorbance at 485 nm. Fig. 5 shows the relative percentages of cells treated with various concentrations of Dex_{10}-ONB-$PMCL_{34}$ or $MDex_7$-ONB-$PMCL_{26}$. Compared with the control, cell viability

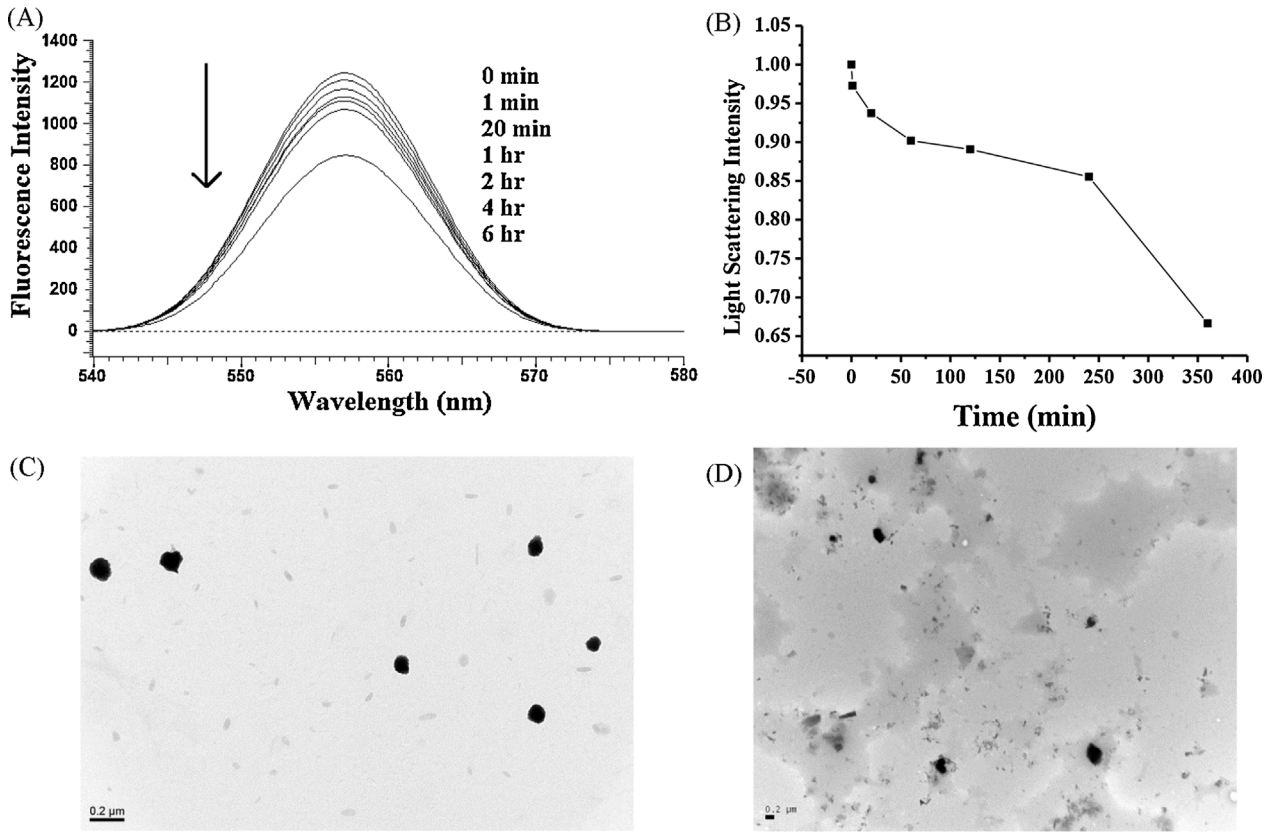

Fig. 3. After UV light exposure (352 nm, 8 W × 8 W) (A) fluorescence spectral changes of Nile Red-loaded Dex_{10}-ONB-$PMCL_{34}$ micelle, (B) normalized fluorescence emission intensity vs. time of the NR-loaded micelle solution, and TEM of Dex_{10}-ONB-$PMCL_{34}$ micelle (C) no irradiation, (D) with irradiation for 6 h.

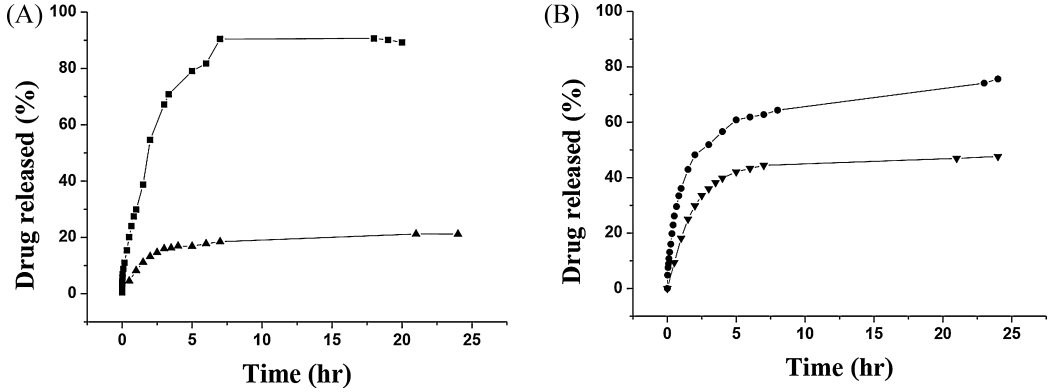

Fig. 4. IMC release from the micelle of (A) Dex_{10}-ONB-$PMCL_{34}$, (B) $MDex_7$-ONB-$PMCL_{26}$ treated in PBS (0.1 M, pH 7.4) at 37 °C: (▲, ▼) without irradiation, (■, ●) under UV irradiation.

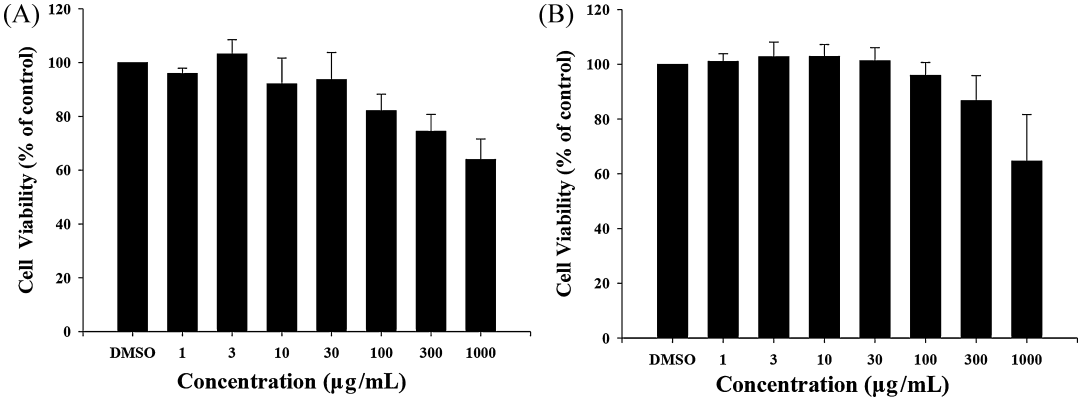

Fig. 5. The cell viabilities of HeLa cells treated with various concentrations of (A) Dex_{10}-ONB-$PMCL_{34}$, (B) $MDex_7$-ONB-$PMCL_{26}$ for 48 h. Data shown as mean ± S.E. ($n = 3$).

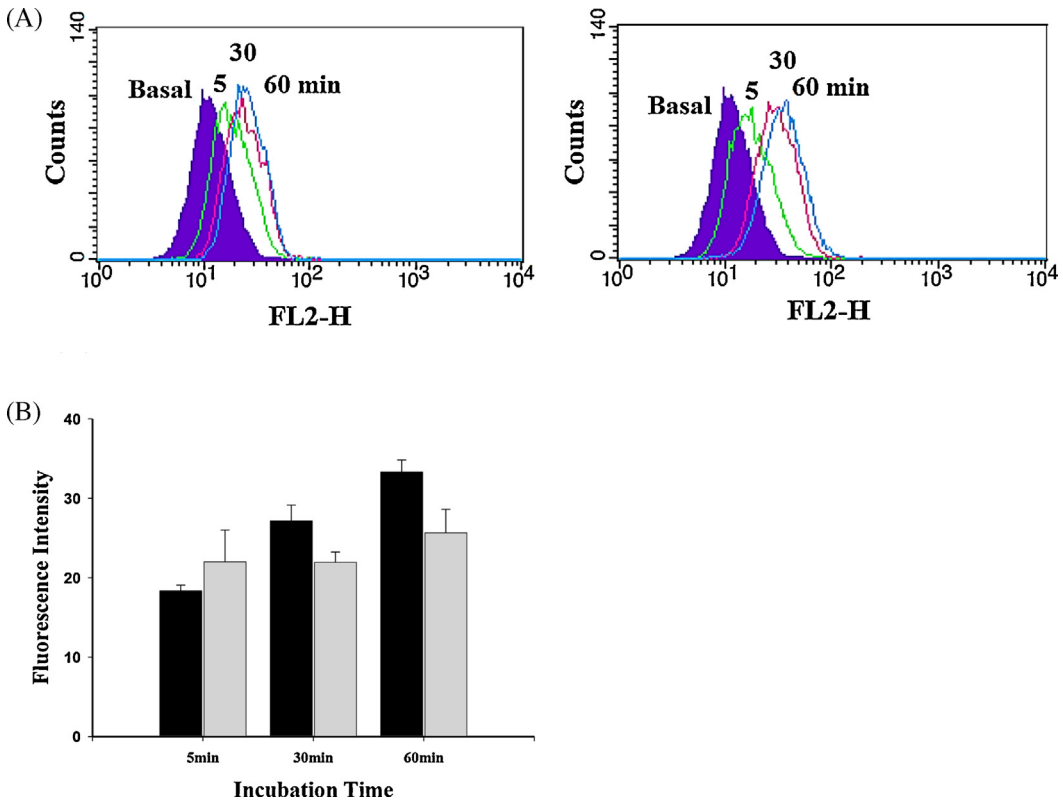

Fig. 6. (A) Flow cytometric histogram profiles of HeLa cells treated with DOX-loaded Dex_{10}-ONB-$PMCL_{34}$ micelles (left) and free DOX (right) for different time intervals (show in minute), (B) Geometric mean fluorescence intensities of free DOX (black) and DOX-loaded Dex_{10}-ONB-$PMCL_{34}$ micelles (gray). Data are shown as mean ± S.E. ($n = 3$).

was higher than 80% at a polymer concentration ranging from 1 to 300 $\mu g\,mL^{-1}$. As the concentration of the polymer above 30 $\mu g\,mL^{-1}$, the cytotoxicity of the Dex_{10}-ONB-$PMCL_{34}$ (Fig. 5A) is larger than the $MDex_7$-ONB-$PMCL_{26}$ (Fig. 5B). Because these polymers exhibit favorable biocompatibility, they may have considerable potential for biomedical applications.

3.7. Cellular uptake profile of doxorubicin-loaded micelles

Amphiphilic polymers can transport drugs through the formation of micelles. Polymer micelles carrying numerous anti-cancer chemotherapies are currently undergoing clinical trials (Oeriemans et al., 2010). In this study, we investigated the drug-carrying ability of polymeric Dex_{10}-ONB-$PMCL_{34}$ micelles by using DOX, which is a potent anti-tumor drug. The self-fluorescent nature of this drug facilitated the identification and quantification of drug-loaded micelles entering cells (Dai et al., 2008; Jin et al., 2011).

DOX-loaded Dex_{10}-ONB-$PMCL_{34}$ micelles were prepared by using dialysis, and recorded the uptake of micelles and free DOX of equal concentration (458.2 ng mL^{-1}) at 5, 30 and 60 min by using flow cytometry (Fig. 6A). In the first 5 min, a feature of Dex_{10}-ONB-$PMCL_{34}$-encapsulated DOX is the relatively fast entry and accumulation into cells (compared to its free-form counterpart). By contrast, the free-form DOX enters and accumulates into cells faster than the DOX-loaded Dex_{10}-ONB-$PMCL_{34}$ at incubation times up to 30–60 min (Liu et al., 2013). The geometric mean fluorescence intensity in HeLa cells treated with DOX-loaded Dex_{10}-ONB-$PMCL_{34}$ was approximately 0.77-fold slower (25.7 vs. 33.5) than in HeLa cells treated with free DOX in the 60-min incubation time (Fig. 6B). Various fluorescence microscopic experiments were conducted to determine the intracellular distributions of DOX-loaded Dex_{10}-ONB-$PMCL_{34}$ micelles or free DOX following cell entry. Fig. 7 shows our results (from left to right) of the nuclear-stained Hoechst 33342, DOX fluorescence, and an overlay of the images. These images indicate that the free DOX and Dex_{10}-ONB-$PMCL_{34}$-encapsulated DOX exhibit distinct temporal and spatial entry patterns. Free DOX accumulated in cells at a substantially faster rate than did the Dex_{10}-ONB-$PMCL_{34}$-encapsulated DOX, with minimal fluorescence after 30 min of treatment, and visible fluorescence after 60 min of treatment (Fig. 7A–C). DOX fluorescence predominantly concentrated in cell nuclei, which could be an inherent tendency of free DOX (Sui, Liu, & Shen, 2011). By contrast, in the HeLa cells treated with DOX-loaded Dex_{10}-ONB-$PMCL_{34}$ for 5, 30, or 60 min, DOX fluorescence was concentrated in the cytoplasm with little to no DOX visible in the nucleus (Fig. 7D–F). These differences could be attributed to the free DOX entering the cells through passive diffusion, whereas the Dex_{10}-ONB-$PMCL_{34}$ micelle-encapsulated DOX penetrated the plasma membrane through endocytosis (Jin et al., 2011; Yan et al., 2011). Another possible reason for these trends is that the endocyted DOX-loaded micelles became trapped in acidic endocytic compartments and gradually released their DOX cargo in a low-pH environment. Because this process is relatively slow, micelle-transported DOX cannot reach the nuclei as fast as free DOX does (Hillarireau & Couvreur, 2009; Ke et al., 2014). Although the uptake of the DOX-loaded Dex_{10}-ONB-$PMCL_{34}$ micelle was slow, slightly more intense nuclear fluorescence was observed in the HeLa cells treated with DOX-loaded Dex_{10}-ONB-$PMCL_{34}$ for 60 min compared with in those treated for 5 min (Fig. 7F and D). Entry of nuclei by DOX confirmed that Dex_{10}-ONB-$PMCL_{34}$ micelle-encapsulated DOX was released and reached its pharmacological target. Low penetration of DOX-loaded Dex_{10}-ONB-$PMCL_{34}$ micelle into the extravascular tumor tissue may be attributed primarily to bulky micelle systems being substantial hindered from penetrating into tumor cell (Sagnella et al., 2013).

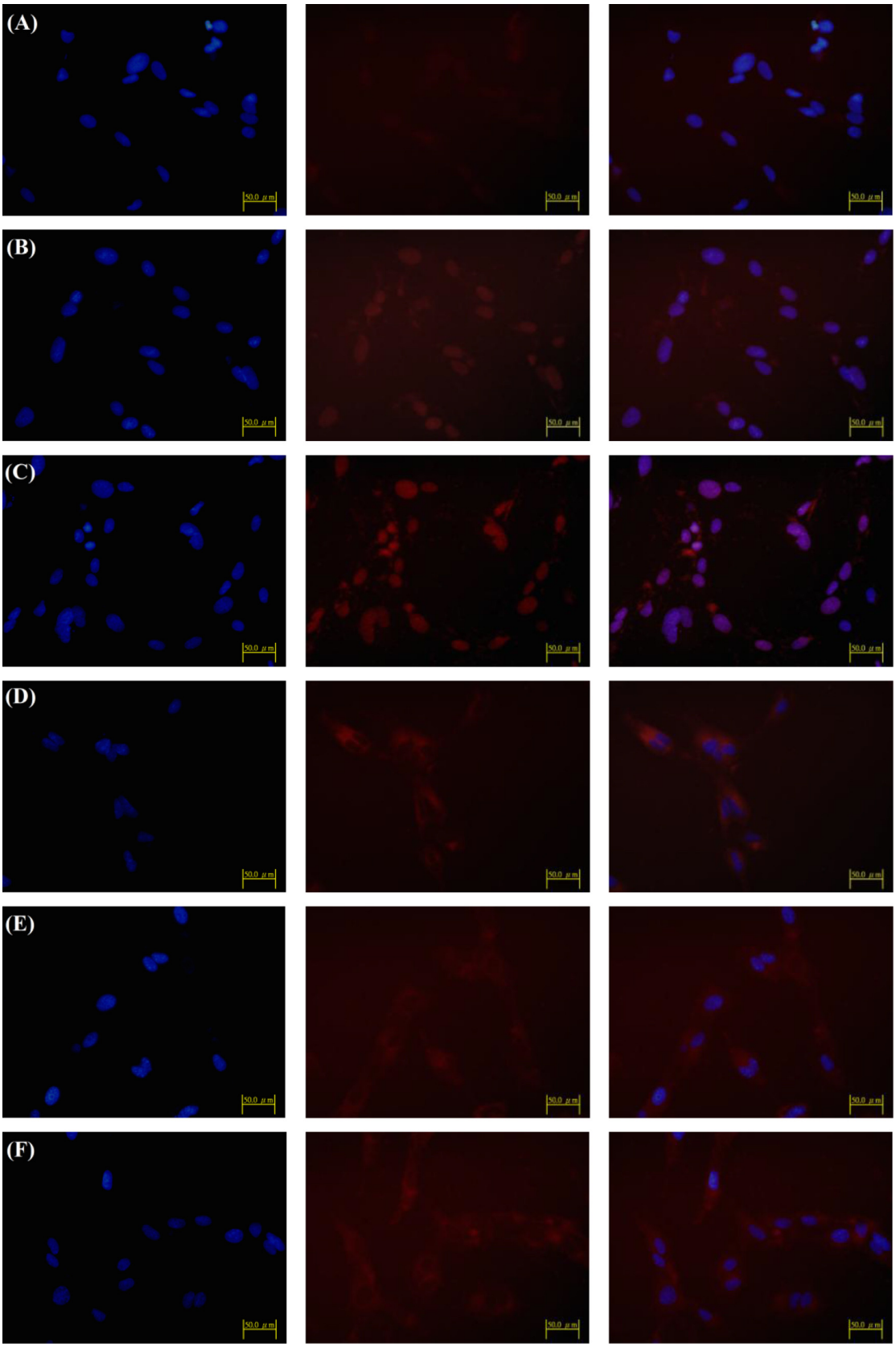

Fig. 7. Fluorescent microscopic images of HeLa cells incubated with free DOX (254.7 ng mL^{-1}) or DOX-loaded micelles for different time intervals: (A) free DOX, 5 min; (B) free DOX, 30 min; (C) free DOX, 60 min; (D) Dex_{10}-ONB-$PMCL_{34}$, 5 min; (E) Dex_{10}-ONB-$PMCL_{34}$, 30 min; (F) Dex_{10}-ONB-$PMCL_{34}$, 60 min. For each row, images for left to right show the cells with Hoechst 33342 nuclear staining, DOX fluorescence, and the merged image (scale bar 50 μm; brightness not proportional to fluorescence intensity).

4. Conclusions

In summary, a family of amphiphilic block copolymers with a photocleavable junction points between the hydrophilic and hydrophobic blocks were synthesized and characterized using ^{1}H NMR, FT-IR, GPC, and DSC. The copolymers formed micelles in an aqueous solution with spherical morphology. Light triggered the burst of particles and release of an encapsulated drug. Cell viability was evaluated in response to these particles at concentrations less than 300 $\mu g\,mL^{-1}$, and observed low toxicity to HeLa cells. Dex-ONB-PMCL-encapsulated DOX can enters and accumulates in cells at a substantially faster rate compared to its free-form counterpart. Therefore, our study results indicate that light-sensitive Dex-ONB-PMCL block copolymers can be used in targeted drug delivery.

Supplementary data

Experimental materials, characterization and spectra of using FT-IR, fluorescence, and GPC, DSC curves of the Dex-ONB-PXCL polymer, as well as TEM photograph of the micelle are shown.

Acknowledgements

The research was supported by grants from National Science Council (NSC 102-2221-E-182-068) and Chang Gung Memorial Hospital (CMRPD5D0011).

Appendix A. Supplementary data

Supplementary data associated with this article can be found, in the online version, at http://dx.doi.org/10.1016/j.carbpol.2014.09.062.

References

Bertrand, O., Poggi, E., Gohy, J. F., & Fustin, C. A. (2014). Functionalized stimuli-responsive nanocages from photocleavable block copolymers. *Macromolecules*, *47*, 183–190.

Bosker, W. T. E., Ágoston, K., Cohen Stuart, M. A., Norde, W., Timmermans, J. W., & Slaghek, T. M. (2003). Synthesis and interfacial behavior of polystyrene-polysaccharide diblock copolymers. *Macromolecules*, *36*, 1982–1987.

Cai, H., Jiang, G., Shen, Z., & Fan, X. (2012). Effects of dendron generation and salt concentration on phase structures of dendritic-linear block copolymers with a semirigid dendron containing PEG tails. *Macromolecules*, *45*, 6176–6184.

Dai, X., Yue, Z., Eccleston, M. E., Swartling, J., Slater, N. K., & Kaminski, C. F. (2008). Fluorescence intensity and lifetime imaging of free and micellar – Encapsulated doxorubicin in living cells. *Nanomedicine*, *4*, 49–56.

Gohy, J. F., & Zhao, Y. (2013). Photo-responsive block copolymer micelles: Design and behavior. *Chemical Society Reviews*, *42*, 7117–7129.

Griffin, D. R., Schlosser, J. L., Lam, S. F., Nguyen, T. H., Maynard, H. D., & Kasko, A. M. (2013). Synthesis of photodegradable macromers for conjugation and release of bioactive molecules. *Biomacromolecules*, *14*, 1199–1207.

Han, D., Tong, X., & Zhao, Y. (2011). Fast photodegradable block copolymer micelles for burst release. *Macromolecules*, *44*, 437–439.

Hernandez, O. S., Soliman, G. M., & Winnik, F. M. (2007). Synthesis, reactivity, and pH-responsive assembly of new double hydrophilic block copolymers of carboxymethyldextran and poly(ethylene glycol). *Polymer*, *48*, 921–930.

Hillarireau, H., & Couvreur, P. (2009). Nanocarriers' entry into the cell: Relevance to drug delivery. *Cellular and Molecular Life Sciences*, *66*, 2873–2896.

Houga, C., Giermanska, J., Lecommandoux, S., Borsail, R., Taton, D., Gnanou, Y., et al. (2009). Micelles and polymersomes obtained by self-assembly of dextran and polystyrene based block copolymers. *Biomacromolecules*, *10*, 32–40.

Hu, X., Tian, J., Liu, T., Zhang, G., & Liu, S. (2013). Photo-triggered release of caged camptothecin prodrugs from dually responsive shell cross-linked micelles. *Macromolecules*, *46*, 6243–6256.

Jin, Y., Song, L., Su, Y., Zhu, L., Peng, Y., Qiu, F., et al. (2011). Oxime linkage: A robust tool for the design of pH-sensitive polymeric drug carriers. *Biomacromolecules*, *12*, 3460–3468.

Kang, M., & Moon, B. (2009). Synthesis of photocleavable poly(styrene-block-ethylene oxide) and its self-assembly into nanoporous thin films. *Macromolecules*, *42*, 455–458.

Ke, X., Coady, D. J., Yang, C., Engler, A. C., Hedrick, J. L., & Yang, Y. Y. (2014). pH-sensitive polycarbonate micelles for enhanced intracellular release of anticancer drugs: A strategy to circumvent multidrug resistance. *Polymer Chemistry*, *5*, 2621–2628.

Kuang, H., Wu, S., Xie, Z., Meng, F., Jing, X., & Huang, Y. (2012). Biodegradable amphiphilic copolymer containing nucleobase: Synthesis, self-assembly in aqueous solutions, and potential use in controlled drug delivery. *Biomacromolecules*, *13*, 3004–3012.

Li, B., Wang, Q., Wang, X., Wang, C., & Jiang, X. (2013). Preparation, drug release and cellular uptake of doxorubicin-loaded dextran-b-poly(ε-caprolactone) nanoparticles. *Carbohydrate Polymers*, *93*, 430–437.

Li, Z., Zhang, D., Weng, J., Chen, B., & Liu, H. (2014). Synthesis and characterization of photochromic azobenzene cellulose ethers. *Carbohydrate Polymers*, *99*, 748–754.

Liu, G., & Dong, C. M. (2012). Photoresponsive poly(s-(o-nitrobenzyl)-L-cysteine)-b-PEO from a L-cysteine N-carboxyanhydride monomer: Synthesis, self-assembly, and phototriggered drug release. *Biomacromolecules*, *13*, 1573–1583.

Liu, J. Y., & Zhang, L. M. (2007). Preparation of a polysaccharide-polyester diblock copolymer and its micellar characteristics. *Carbohydrate Polymers*, *69*, 196–201.

Liu, P., Shi, B., Yue, C., Gao, G., Li, P., Yi, H., et al. (2013). Dextran-based redox-responsive doxorubicin prodrug micelles for overcoming multidrug resistance. *Polymer Chemistry*, *4*, 5793–5799.

Lv, C., Wang, Z., Wang, P., & Tang, X. (2012). Photodegradable polyurethane self-assembled nanoparticles for photocontrollable release. *Langmuir*, *28*, 9387–9394.

Oeriemans, C., Bult, W., Bos, M., Storm, G., Nijsen, J. F., & Hennink, W. E. (2010). Polymeric micelles in anticancer therapy: Targeting imaging and triggered release. *Pharmaceutical Research*, *27*, 2569–2589.

Otsuka, I., Fuchise, K., Halila, S., Fort, S., Aissou, K., Pignot-Paintrand, I., et al. (2010). Thermoresponsive vesicular morphologies obtained by self-assemblies of hybrid oligosaccharide-block-poly N-isopropylacrylamide copolymer systems. *Langmuir*, *26*, 2325–2332.

Peng, K., Tomatsu, I., Broke, B., Cui, C., Korobko, A. V., Noort, J., et al. (2011). Dextran based photodegradable hydrogels formed via a Michael addition. *Soft Matter*, *7*, 4881–4887.

Peng, K. Y., Wang, S. W., Hua, M. Y., & Lee, R. S. (2013). Amphiphilic photocleavable block copolymers based on monomethyl poly(ethylene glycol) and poly(4-substituted-ε-caprolactone): Synthesis, characterization, and cellular uptake. *RSC Advances*, *3*, 18453–18463.

Peng, K. Y., Wang, S. W., & Lee, R. S. (2013). Amphiphilic diblock copolymers based on poly(2-ethyl-2-oxazoline) and poly(4-substituted-ε-caprolactone): Synthesis, characterization, and cellular uptake. *Journal of Polymer Science Part A: Polymer Chemistry*, *51*, 2769–2781.

Sagnella, S. M., Duong, H., MacMillan, A., Boyer, C., Whan, R., McCarroll, J. A., et al. (2013). Dextran-based doxorubicin nanocarriers with improved tumor penetration. *Biomacromolecules*, *15*, 262–275.

Schumers, J. M., Fustin, C. A., & Gohy, J. F. (2010). Light-responsive block copolymers. *Macromolecular Rapid Communications*, *31*, 1588–1607.

Schumers, J. M., Gohy, J. F., & Fustin, C. A. (2010). A versatile strategy for the synthesis of block copolymers bearing a photocleavable junction. *Polymer Chemistry*, *1*, 161–163.

Sui, M., Liu, W., & Shen, Y. (2011). Nuclear drug delivery for cancer chemotherapy. *Journal of Controlled Release*, *155*, 227–236.

Wang, B., Chen, K., Yang, R., Yang, F., & Liu, J. (2014). Stimulus-responsive polymeric micelles for the light-triggered release of drugs. *Carbohydrate Polymers*, *103*, 510–519.

Xu, N., Lu, F. Z., Du, F. S., & Li, Z. C. (2007). Synthesis of saccharide-terminated poly(ε-caprolactone) via Michael addition and click chemistry. *Macromolecular Chemistry and Physics*, *208*, 730–738.

Yan, J., Ye, Z., Chen, M., Liu, Z., Xiao, Y., Zhang, Y., et al. (2011). Fine tuning micellar core-forming block of poly(ethylene glycol)-block-poly(ε-caprolactone) amphiphilic copolymers based on chemical modification for the solubilization and delivery of doxorubicin. *Biomacromolecules*, *12*, 2562–2572.

Yang, C., Ebrahim Attia, A. B., Tan, J. P. K., Ke, X., Gao, S., Hedrick, J. L., et al. (2012). The role of non-covalent interactions in anticancer drug loading and kinetic stability of polymeric micelles. *Biomaterials*, *33*, 2971–2979.

Zhao, H., Gu, W., Thielke, M. W., Sterner, E., Tsai, T., Russell, T. P., et al. (2013). Functionalized nanoporous thin films and fibers from photocleavable block copolymers featuring activated esters. *Macromolecules*, *46*, 5195–5201.

Zhao, H., Sterner, E. S., Coughlin, E. B., & Theato, P. (2012). O-nitrobenzyl alcohol derivatives: Opportunities in polymer and materials science. *Macromolecules*, *45*, 1723–1736.